Local structure around cations in the T'-type Nd(Ce) based superconducting system: an EXAFS study

1997 J. Phys.: Condens. Matter 9 9695

(http://iopscience.iop.org/0953-8984/9/44/023)

J. Phys.: Condens. Matter **9** (1997) 9695–9714. Printed in the UK PII: S0953-8984(97)81330-6

Local structure around cations in the T′-type Nd(Ce) based superconducting system: an EXAFS study

B D Padalia†, Gunadhor S Okram†, Om Prakash‡, S J Gurman§ and J C Amiss‖

† Department of Physics, Indian Institute of Technology, Powai, Mumbai 400076, India
‡ Department of Metallurgical Engineering and Materials Science, Indian Institute of Technology, Powai, Mumbai 400076, India
§ Department of Physics and Astronomy, University of Leicester, Leicester LE1 7RH, UK
‖ BMS, Sheffield Hallam University, Sheffield S1 1WB, UK

Received 27 January 1997, in final form 25 April 1997

Abstract. EXAFS measurements on all the cations in Nd_2CuO_4, $Nd_{2-x}Ce_xCuO_y$ (NCCO) and $Nd_{1.82-z}A_zCe_{0.18}CuO_y$ (NACCO), A=Sr, Ca or Ba, $x = 0.06$ or 0.18, have been made using synchrotron radiation. Bond lengths (R), coordination numbers (N) and Debye–Waller factors (σ^2) have been obtained from the EXAFS analysis. The curved wave theory in the single-scattering approximation and the small-atom multiple-scattering theory have been applied to experimental EXAFS data and it is found that the latter gives a better fit. The CuO_2 plane contains a strong multiple-scattering contribution. Further, all the dopants (Ce, Sr, Ca and Ba) occupy the Nd site without affecting the basic T′ structure. Doping affects the local structure around the substituents as reflected by the changes in R and σ^2 values. The observed CuO_2 layer distortion (or large Cu–O–Cu angle deviation from linearity, 180°) is found to have an adverse effect on T_c as observed in Ca or Ba doped NACCO samples.

Further, it is realized that critical levels of charge carriers, oxygen vacancies and CuO_2 planar effects have a strong influence on the SC behaviour of the T′-type electron doped cuprates.

1. Introduction

The electron doped, T′-type $R_{2-x}Ce_xCuO_y$ (R = Pr, Nd, Sm and Eu) superconducting (SC) system [1, 2] has attracted much attention in recent years [3–10]. It is well known that superconductivity in the $Nd_{2-x}Ce_xCuO_y$ (NCCO) system is induced by partial substitution of Ce at the Nd site in Nd_2CuO_4 followed by a reduction process. Electrons are, thus, doped in the CuO_2 layers through Ce^{4+} substitution and partial oxygen removal. It appears that critical levels of both the charge carriers and the oxygen vacancies are indispensable for exhibition of T_c in the T′-type cuprates [11]. Further, some of the observations on the NCCO system are that (i) superconductivity occurs in a narrow Ce range, $0.14 < x < 0.18$, (ii) the reduction process is mandatory for the exhibition of T_c and (iii) relatively low values of T_c (onset) $\leqslant$24 K [1, 2, 12]. Although various structure–property aspects of T′ SC cuprates have been discussed by several investigators [1–17], the mechanism of superconductivity is still not adequately understood. It is desirable to generate more information on structural changes due to doping in the Nd(Ce) based T′-type cuprates. We have, therefore, planned to carry out systematic studies of the NCCO compounds using various techniques.

A refined phase diagram has been drawn for the T′-type NCCO system in the range $0.120 < x < 0.190$. The highest T_c (onset) ∼24 K is found to be in a narrow Ce range

0953-8984/97/449695+20$19.50

$0.145 \leqslant x \leqslant 0.150$ and for $x \geqslant 0.18$ the sample becomes non-SC [12]. Interestingly, superconductivity in the Ce rich ($x = 0.18$) T′-type NCCO compound has been revived by doping it with alkaline earth elements [7]. The thermoelectric power (TEP) studies on our NCCO $x < 0.18$ compounds have indicated a negative sign of TEP, suggesting electron conduction [18]. A direct evidence for the local oxygen non-stoichiometry in NCCO SC samples was obtained through a high-resolution analytical SEM technique. A correlation between oxygen vacancies, Ce content (x) and appearance of T_c in the T′-type NCCO system was established [11].

The local structure is known to have a strong bearing on the SC properties of cuprate materials. It is, therefore, of interest to see how (i) doping of mixed-valence Ce alone ($x \leqslant 0.18$) and (ii) co-doping of divalent Ca, Ba or Sr with Ce ($x = 0.18$) in Nd_2CuO_4 affect the local structure and, thereby, influence the SC behaviour of the T′-type compounds. Since the extended x-ray absorption fine structure (EXAFS) is recognized as a powerful tool for studies of the local structure in high-T_c SC materials [19–22], a systematic EXAFS study of the T′-type SC compounds has been carried out using synchrotron radiation facilities at Daresbury, UK. Interesting results on the local structure of dopants (as well as host ions) have emerged from the analysis of the EXAFS data fitted with the curved wave theory including multiple-scattering effects. A brief report on a part of this work has been presented elsewhere [19]. Here, we discuss in detail the results of our EXAFS measurements on all the cations in $Nd_{1.85}Ce_{0.15}CuO_y$ (NCCO), reduced as well as oxygenated, and $Nd_{1.82-z}A_zCe_{0.18}CuO_y$ (NACCO), A = Ca, Ba or Sr, $z = 0.06$ or 0.18 along with the reference compound, Nd_2CuO_4. Although there are several reports available on the neutron (and x-ray) diffraction studies of the T′-type structure [16, 23–27], relatively little attention has been paid to the use of EXAFS to obtain information on the local structure. This is, perhaps, the first detailed report on the EXAFS studies of the local structure in the T′-type NCCO and NACCO SC compounds (i.e. electron doped SC systems).

2. Sample preparation

The samples of nominal compositions Nd_2CuO_4, $Nd_{2-x}Ce_xCuO_y$ ($x = 0$, 0.15) and $Nd_{1.82-z}A_zCe_{0.18}CuO_y$ (NACCO), A = Ca, Ba or Sr, $z = 0.06$ or 0.18, were synthesized by the solid state reaction route under different processing conditions. The samples were quenched and subsequently annealed in Ar ambient. The details are given elsewhere [7, 15].

The powder x-ray diffraction (XRD) patterns were recorded on a Philips x-ray diffractometer using Cu Kα radiation. The scanning speed was maintained at 0.5° min^{-1}. The iodometric titration method [8] was used to estimate the oxygen content (y) of the samples. Argon atmosphere was maintained during titrations to check the absorption of oxygen from the atmosphere. The estimated error in y was found to be ± 0.01. The ac susceptibility measurements on T_c (onset) were conducted with a Sumitomo SCR204T set-up, at a frequency of 313 Hz and a field of $\sim$52 mOe in the temperature range 300–$\sim$12 K. The resistivity, $\rho(T)$, of the samples was measured by a dc four-probe method in the temperature range 300–5 K. Microstructure examination and high-resolution microprobe analysis were carried out using a Cameca SU-SEM probe analytical SEM [11].

3. Experimental details

EXAFS measurements were made on a large number of samples of $Nd_{2-x}Ce_xCuO_y$ (NCCO) and $Nd_{1.82-z}A_zCe_{0.18}CuO_y$ (NACCO) and the reference compound, Nd_2CuO_4, using the

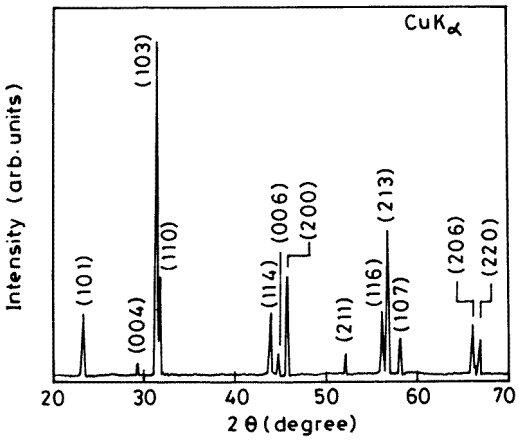

Figure 1. The XRD pattern for the reduced $Nd_{1.85}Ce_{0.15}CuO_y$ sample.

2 GeV Synchrotron radiation source (SRS) Daresbury Laboratory, UK. Beam current during data collection ranged between 150 and 250 mA. All experiments were performed on finely powdered samples mounted on Scotch tape. These were clamped to the cold finger of a liquid nitrogen Dewar; the sample temperatures were ∼100 K.

Absorption measurements for the major components, Cu (K edge) and Nd (L_3 edge) were made in transmission mode on station 7.1. This station has an Si(111) double-crystal monochromator to define the x-ray energy; harmonic rejection was set at 50%. The x-ray flux before and after absorption by the sample was measured using gas filled ion chambers. Data were obtained over an energy range corresponding to photoelectron wavenumbers of 1–20 $Å^{-1}$ with a close scan in the edge region. Four to five spectra, each taking about 30 min, were averaged to give the final data set.

Data for the minor components, Ce (L_3 edge), Ba (L_3 edge), Ca (K edge) and Sr (K edge) were measured in fluorescence mode on station 8.1 or 9.2. Harmonic rejection from the channel-cut Si(220) monochromators was again set at 50%. Signal detection was by a 13-element Canberra solid state detector with energy window set to pickup the appropriate atom fluorescence x-ray peak. Signal to background ratios were about ten. Again, four or five spectra, each taking about 40 min, were averaged to given the final data set which had a fluorescence count of 10^6–10^7 photons/data point. Data were usually obtained out to a photoelectron wavenumber of 15 $Å^{-1}$.

3.1. Data analysis

The data sets from the experimental station were calibrated and averaged using the EXCALIB program of Morrell *et al* [28]. This produces, as output, data proportional to the linear absorption coefficient or the ratio of the fluorescence signal to the incident x-ray flux, as appropriate, as a function of x-ray energy. For background subtraction we used the EXBACK program by the same workers to fit low-order polynomials to the pre- and post-edge data to represent the smooth atomic background. These were then subtracted in the usual way to give the EXAFS function $\chi(k)$.

Structural information was obtained by multi-parameter fitting of the experimental EXAFS data to an EXAFS function calculated using the single-scattering curved wave

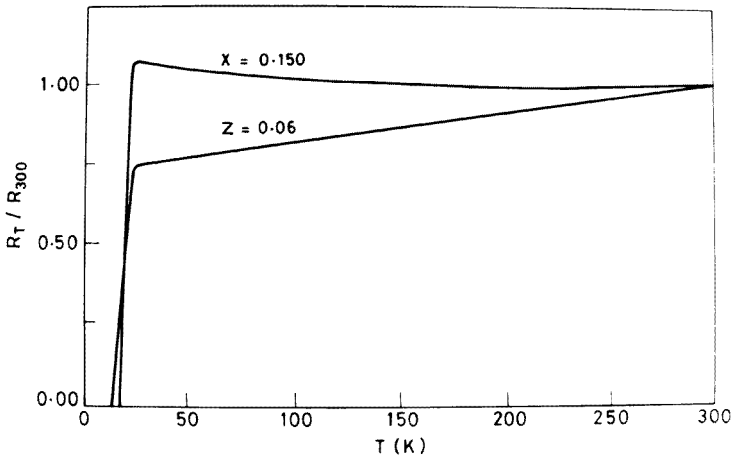

Figure 2. Normalized resistance $R(T)/R(300)$–T plots for the reduced $Nd_{1.85}Ce_{0.15}CuO_y$ and $Nd_{1.82-z}Sr_zCe_{0.18}CuO_y$ ($z = 0.06$) samples.

theory [29]. The program used was the standard Daresbury package EXCURV92 [30]. For successful application of the theory it is necessary to use a reliable set of scattering data. The scattering phase shifts used were calculated within the program using a Hedin–Lundqvist exchange and correlation potential [31]. This is a complex, energy-dependent potential which gives good scattering factors, including inelastic effects, for photoelectrons. The program also includes a factor for the core-hole lifetime. In the present work the factor $A(k)$, which accounts for amplitude reduction from multiple-excitation effects (and is close to unity for the Hedin–Lundqvist potential) was derived from spectra for model compounds. These were also used to check the phase shifts. In the case of the Cu K edge, we also analysed the data using the small-atom approximation [32] which is included as an option in EXCURV92. This allows the inclusion of multiple-scattering contributions in on-line refinement. In these contributions, bond angles (e.g. Cu–O–Cu) are also treated as fitting parameters.

The EXCURV92 fitting routine uses a non-linear least-squares fit of the theory to the experimental EXAFS data. The variable parameters are the interatomic distances R_j and the energy offset E_F, which together fix the phase of $\chi(k)$, the coordination numbers N_j and the mean square variations in distance σ_j^2. These latter parameters control the amplitude of $\chi(k)$. When multiple-scattering contributions are included information may also be obtained on the angles between the various legs of the scattering path [32]. The data ranges used in the fits were generally 5-600 eV above the absorption edge, corresponding to a k range of 2–13 Å^{-1}. The program varies selected parameters until a minimum is obtained in the fit index, FI, defined by

$$\text{FI} = \frac{1}{N_p}\sum_{i=1}^{N_p}\{[\chi(\text{calc}) - \chi_i(\text{exp})]k^n\}^2$$

where N_p is the number of data points and n is a k-weighting factor used to equalize the contribution of all the points to FI; $n = 3$ was used throughout this work.

A non-trivial problem encountered when using this type of curve fitting approach is the estimation of the uncertainties in the fitted parameters. This problem is complicated

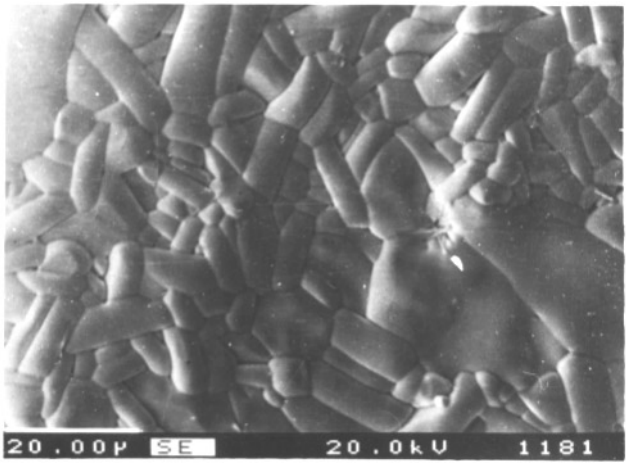

Figure 3. A typical micrograph of an SC NCCO sample.

Table 1. The computed lattice parameters from XRD and T_c (onset) from R–T data.

Composition	a (Å)	c (Å)	V (Å^3)	T_c (onset) (K)
Nd_2CuO_4	3.9380(6)	12.174(2)	188.79	—
$Nd_{1.85}Ce_{0.15}CuO_{3.97}$	3.9500(1)	12.092(2)	188.66	24
$Nd_{1.76}Sr_{0.06}Ce_{0.18}CuO_{3.99}$	3.9476(7)	12.079(3)	188.23	23
$Nd_{1.76}Ca_{0.06}Ce_{0.18}CuO_y$	3.925(3)	11.973(9)	184.45	21
$Nd_{1.76}Ba_{0.06}Ce_{0.18}CuO_y$	3.98(1)	12.2(1)	193.25	19

by the presence of correlation between parameters, especially the pairs (R_j, E_F) and (N_j, σ_j^2) introduced by the limited data range. We have used the statistical test described by Joyner *et al* [33] to estimate these uncertainties. This test, which forms an integral part of EXCURV92, provides a plot of the 95% significance region ($\pm 2\ \sigma$ uncertainty) on a contour map of FI when this is plotted as a function of two correlated variables. It is these $\pm 2\ \sigma$ uncertainties which are given in the tables of our structural parameters. This test may also be used to determine whether a shell of scattering atoms gives a significant contribution to the fit: only significant shells are included in our tables. In particular, a possible long oxygen distance at about 2.3 Å from the copper atom was rarely found to give a significant improvement to the fit to the Cu K edge data.

4. Results and discussion

XRD patterns show that each sample of the compositions $Nd_{2-x}Ce_xCuO_y$ ($x = 0$, 0.15) and $Nd_{1.82-z}A_zCe_{0.18}CuO_y$, A=Sr, Ca or Ba, $z = 0.06$ or 0.18 has monophasic T′ structure. The powder XRD pattern of a reduced NCCO sample with $x = 0.15$ is shown in figure 1, indicating no impurity lines. The $R(T)/R(300)$–T plots for the SC NCCO and NACCO (A = Sr, $z = 0.06$) samples are shown in figure 2. The computed lattice parameters along with the measured T_c values are given in table 1. The T_c (onset) values from the ac susceptibility data for SC NCCO samples [12] match well with those obtained from R against T. The SEM micrographs reveal fairly uniform, well grown grains (see, for example, figure 3).

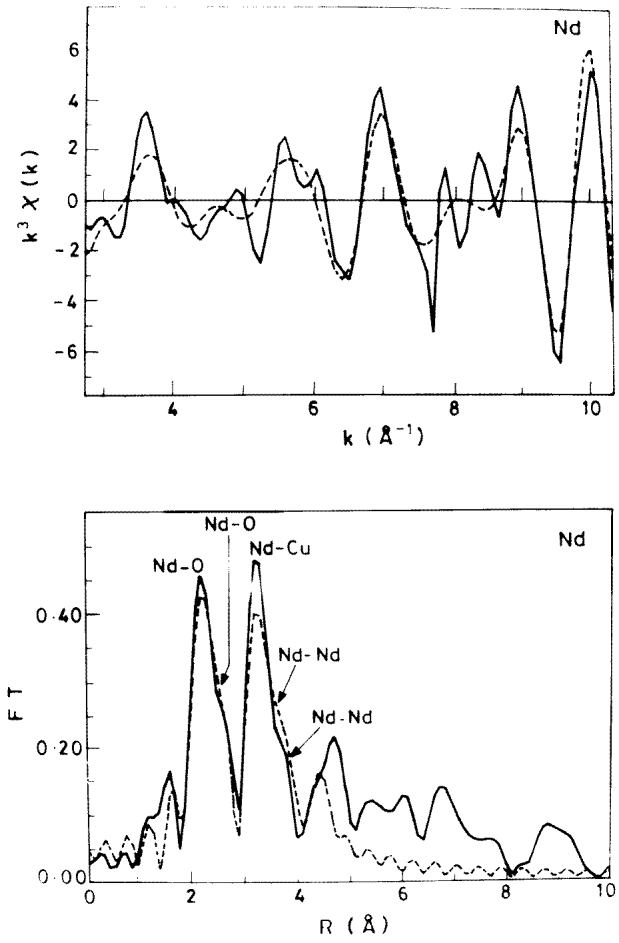

Figure 4. EXAFS (top) and FT (bottom) of Nd in Nd_2CuO_4.

4.1. EXAFS

4.1.1. Nd_2CuO_4: the reference compound. Figures 4 and 5 show the background subtracted and k^3-weighted EXAFS function, $\chi(k)$, for Nd and Cu in Nd_2CuO_4 along with the corresponding Fourier transforms (FTs). The theoretical fits are represented by broken curves while the continuous curves correspond to experimental EXAFS data. The FTs are phase corrected and, therefore, the peaks appear at the true interatomic distances (R). The coordination numbers (N) and the Debye–Waller factors (mean square deviations, σ^2) are obtained from EXAFS analysis. The R, N and σ^2 values for Nd_2CuO_4 are given in table 2. For comparison, the R and N values as determined from x-ray and neutron diffraction [23–25] are included in the table. The absolute uncertainties in EXAFS R, N and σ^2 values are ± 0.02 Å, ± 1 and $\pm 50 \times 10^{-4}$ Å^2, respectively. The uncertainties ($\pm 2\sigma$) quoted are of the 95% confidence limits. The Debye–Waller factors (σ^2) for Cu–O bonds are found to be small (much smaller than those of the corresponding Nd–O bonds). This implies that CuO_2 square planar unit in Nd_2CuO_4 is very rigid.

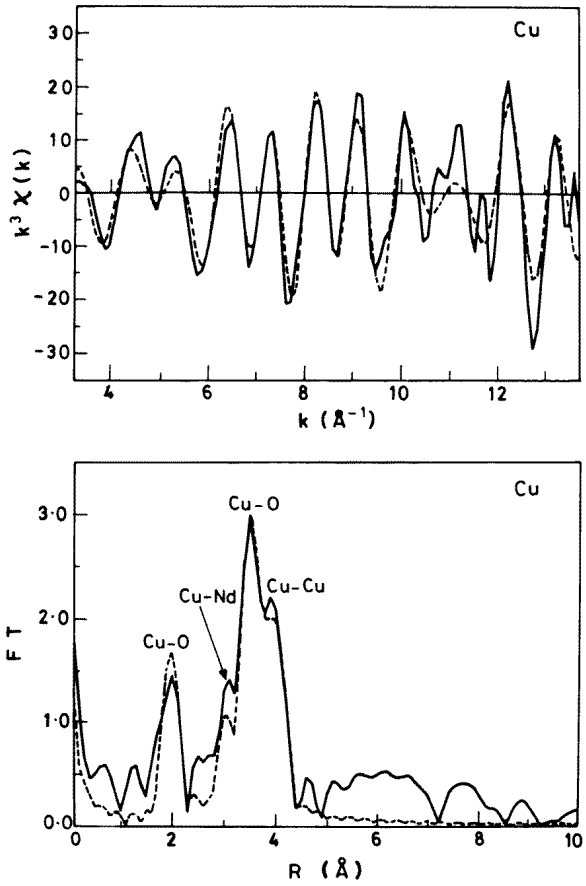

Figure 5. EXAFS (top) and FT (bottom) of Cu in Nd_2CuO_4.

Further, the Cu–O–Cu angle (in the CuO_2 plane) iterates to $177 \pm 10^\circ$ as calculated using small-atom multiple-scattering theory for four shells (see table 2); the oxygen shell at $\sim$3.6 Å is poorly defined due to overlapping with the Nd shell at 3.71 ± 0.02 Å. Floating *N* and *R* values are all consistent with the crystallographic data [23–25]. The present Cu K edge EXAFS features for Nd_2CuO_4 are similar to those reported by others [22, 34]. We have, however, found no clear evidence of interstitial/apical oxygen in the case of Nd_2CuO_4 as reported by Ghigna *et al* [34] and Radaelli *et al* [27]. The absence of apical oxygen is also reported by Marin *et al* [35]. The consistency check shown in table 2 indicates a reasonable fit for the constrained *N* values, while the fits for the unconstrained *N* values are remarkably good. Thus, the test on Nd_2CuO_4 clearly reveals the accuracy in the present experimental EXAFS data collected and their theoretical fittings.

4.1.2. The NCCO system: the effect of Ce doping. It is noted that the EXAFS features of the Nd L_3 edge and Cu K edge (not reproduced here) in the Ce substituted NCCO samples are similar to those of EXAFS of Nd and Cu in Nd_2CuO_4 (figures 4 and 5). The EXAFS and FT of the Ce dopant in the NCCO compound are shown in figure 6. The FTs of the EXAFS

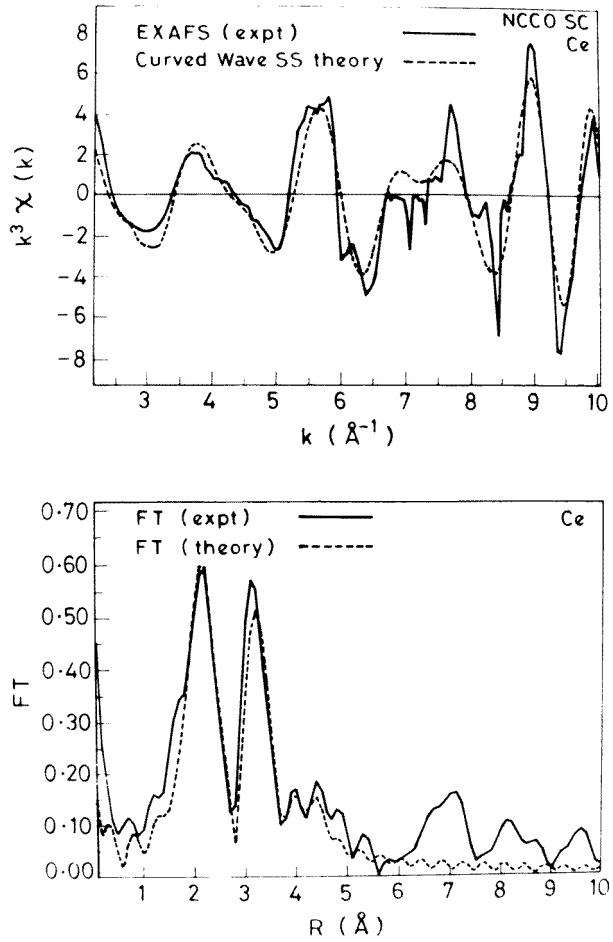

Figure 6. EXAFS (top) and FT (bottom) of Ce in the reduced SC $Nd_{1.85}Ce_{0.15}CuO_{3.97}$ sample.

of Cu and Ce in the reduced NCCO, along with those of Cu and Nd in the Nd_2CuO_4, for the purpose of comparison, are shown in figure 7. There are five peaks corresponding to the five shells (near neighbours). These features are similar to those reported by Tan Zhengquan *et al* [22]. On fitting the curved wave theory in the single-scattering (SS) approximation as well as the small-atom multiple-scattering (MS) theory to the experimental EXAFS data, it was found that the MS theory gave a better fit. The R, N and σ^2 values are given in table 3 for the oxygenated (non-SC) and reduced (SC) NCCO samples. It is seen from tables 2 and 3 that the first shell mean Cu–O(1) bond distance (O(1) represents the planar oxygen) is not affected by Ce substitution in Nd_2CuO_4. Further, all the coordinations for Nd(Ce) in the non-SC NCCO are consistent with four. The mean Cu–Cu bond distance along the a (or b) axis is also constant (at 3.93 ± 0.02 Å) in line with the crystallographic data; a is slightly shorter compared to that in Nd_2CuO_4 [23–25]. The results show that the basic T′ structure is unaffected by Ce doping in Nd_2CuO_4. However, the σ^2 values (table 3) for Cu–O bonds in the Ce doped SC and non-SC NCCO samples are affected significantly. This implies a decrease in the rigidity of Cu–O bond and an increase in local disorder/defects on Ce doping.

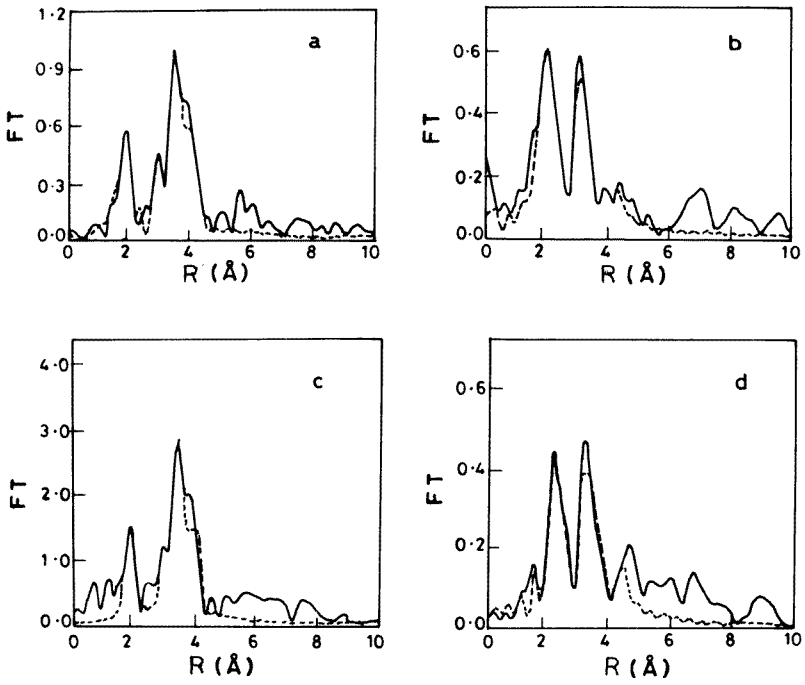

Figure 7. FTs of EXAFS of (a) Cu and (b) Ce ions in reduced SC $Nd_{1.85}Ce_{0.15}CuO_{3.97}$ and for comparison (c) Cu and (d) Nd in Nd_2CuO_4. Experimental data are represented by continuous (——) curves and theoretical fits by dashed (– – –) curves.

Interestingly, the Cu environment in the oxygenated (non-SC) $Nd_{1.85}Ce_{0.15}CuO_{4.05}$ is found to be different from that in the reduced SC $Nd_{1.85}Ce_{0.15}CuO_{3.97}$ samples. This observation suggests that the local structure is affected even by small changes in oxygen content in NCCO samples. This is reflected in the lower values of N in both the in-plane (Cu–O(1)) ($N < 4$) and the out-of-plane (Cu–O(2)) ($N < 8$) oxygen neighbours as well as large values of σ^2 (see table 3) for the reduced SC NCCO samples. The depletion of relatively more oxygen from the CuO_2 plane ($N < 4$) can cause a reduction of a fraction of the $Cu^{2+}(3d^9)$ to $Cu^{+}(3d^{10})$. If so, this has far-reaching consequences pertaining to the mechanism of charge transfer and conductivity/superconductivity in the CuO_2 plane. Our Cu K-XANES results, indeed, show a fraction of Cu^{2+} going to Cu^{+} on reduction of the NCCO samples [36]. It is noted that the second-shell Nd–O(1) bond distances and also other bond lengths in the Ce doped samples contract slightly. In general, a rise in σ^2 is observed. The overall environment around Nd, nevertheless, remains almost unchanged.

In NCCO, the first-shell Ce–O(2) bond distance (2.21 Å) is shorter than that of the Nd–O(2) bond (O(2) represents the out-of-plane oxygen). This is consistent with the EXAFS results reported on $x = 0.20$ NCCO samples by Ghigna *et al* [6]. The neutron and x-ray diffraction data on the NCCO system, however, show a single value [23–26] for Nd/Ce–O(2). These techniques could not resolve Ce–O(2) from Nd–O(2), probably due to limitations of the probes. Further, the shorter Ce–O(2) bond is rather ordered (lower σ^2 value) while the larger Ce–O(1) bond ($R = 2.61$ Å) is more disordered (less rigid) than the corresponding Nd–O(1) bond. This suggests that the Cu–O layer structure in the vicinity of Ce is perturbed. However, the Nd environment in the SC NCCO shows no visible

Table 2. Near-neighbour distances (R), coordination numbers (N) and Debye–Waller factors (mean square distances, σ^2) obtained from EXAFS analysis for Nd_2CuO_4. Co-ordination numbers were held fixed unless an uncertainty is indicated.

		EXAFS (present)			XRD	
	Bond	N	R (±0.02 Å)	σ^2 (10^{-4} Å^2)	N	R (±0.02 Å)
Nd environment	Nd–O(2)	4	2.32	63 ± 20	4	2.322
	Nd–O(1)	4	2.67	80 ± 30	4	2.670
	Nd–Cu	4	3.33	65 ± 15	4	—
	Nd–Nd	4	3.71	50 ± 15	4	—
	Nd–Nd	4	3.94	50 ± 20	4	3.944
Cu environment	Cu–O(1)	4	1.97	9 ± 12	4	1.969
	Cu–Nd	8	3.30	30 ± 15	8	3.318
	Cu–O(2)	8	3.61	30 ± 60	8	—
	Cu–Cu	4	3.93	50 ± 10	4	—
Consistency check						
	Bond	N	R (±0.02 Å)	σ^2 (10^{-4} Å^2)	Comments	
Unconstrained	Cu–Nd	9 ± 5	3.31	85 ± 50	good	
	Nd–Cu	7 ± 4	3.32	110 ± 50		
Constrained	Cu–Nd	8	3.30	30 ± 15	reasonable	
	Nd–Cu	4	3.33	65 ± 15		

O(1), in-plane; O(2), out-of-plane oxygen [24].

changes in the first-shell Nd–O(2) distance and the N values *vis-à-vis* in Nd_2CuO_4. Thus, Ce directly substitutes for Nd. In the present results, Ce near-neighbour distances are, in general, slightly less (except the first-shell Ce–O distances) than those reported by Ghigna *et al* [6]. This can be attributed to the higher Ce content and the associated lattice oxygen in their $x = 0.20$ (non-SC) NCCO samples.

4.1.3. The NACCO system: the effect of co-doping of Sr, Ca or Ba with Ce. The EXAFS features of the Nd L_3 edge and Cu K edge in the co-doped samples, $Nd_{1.82-z}A_zCe_{0.18}CuO_y$ (NACCO), A = Sr, Ca or Ba, $z = 0.06$ or 0.18, are similar to those of Nd and Cu in Nd_2CuO_4, and, hence, are not reproduced here. However, the typical EXAFS of the dopants Sr ($z = 0.06$) and Ca ($z = 0.18$) along with Ce (0.18) in NACCO compounds are shown in figures 8–10. The FTs of EXAFS of all the cations (except Ba) in selected NACCO compounds along with those of NCCO and Nd_2CuO_4 (for the purpose of comparison) are grouped together in figures 11 and 12.

The R, N and σ^2 values for the NACCO compounds obtained from the EXAFS analysis are given in table 4. It is apparent from the data that the mean environments of Nd and Cu are not changed on co-doping. The EXAFS results on NACCO compounds compare well with the crystallographic data on Nd_2CuO_4 [23–25]. The Cu–O(1) bond distance ($R = 1.96 \pm 0.02$ Å) in the CuO_2 plane remains the same in all the samples. This Cu–O(1) distance matches with sum of the ionic radii of Cu^{2+} (0.72 Å) and O^{2-} (1.32 Å) [37]. The first-shell Nd–O(2) distance (2.31 ± 0.02 Å) also matches with the ionic radii Nd^{3+} (1.00 Å) and O^{2-} (1.32 Å). Further, four oxygen O(1) ions lie between the Cu ions in the

Table 3. N, R and σ^2 values as obtained from the EXAFS analysis for $Nd_{1.85}Ce_{0.15}CuO_y$ (NCCO). Co-ordination numbers were held fixed unless an uncertainty is indicated.

	$Nd_{1.85}Ce_{0.15}CuO_{3.97}$ (reduced SC)				$Nd_{1.85}Ce_{0.15}CuO_{4.05}$ (oxygenated non-SC)			
	Bond	N	R (±0.02 Å)	$\sigma 2$ (10^{-4} Å^2)	Bond	N	R (±0.02 Å)	σ^2 (10^{-4} Å^2)
Cu environment								
Single-scattering curve wave theory								
	Cu–O(1)	3.0 ± 1.0	1.96	90 ± 60	Cu–O(1)	5 ± 2	1.94	40 ± 40
	Cu–Nd	6.3 ± 2.0	3.29	65 ± 20	Cu–Nd	7 ± 2.5	3.30	75 ± 20
Multiple-scattering, small-atom approximation								
	Cu–O(1)	2.6 ± 1.0	1.94	70 ± 50	Cu–O(1)	4	1.94	70 ± 50
	Cu–Nd	8.0 ± 2.0	3.28	40 ± 20	Cu–Nd	8	3.31	55 ± 10
	Cu–O(2)	6.0 ± 3.0	3.34	20 ± 150	Cu–O(2)	8	3.31	500 ± 500
	Cu–Cu	2.6 ± 1.0	3.92	25 ± 25	Cu–Cu	4	3.95	-10 ± 20
Consistency check (unconstrained)								
	Cu–Nd	11 ± 3.0	3.31	55 ± 10				
	Nd–Cu	2.5 ± 2.5	3.29	11 ± 70				
	Ce–Cu	4.3 ± 2.4	3.34	50 ± 40				
	Nd environment				Ce environment			
	Bond	N	R (±0.02 Å)	$\sigma 2$ (10^{-4} Å^2)	Bond	N	R (±0.02 Å)	σ^2 (10^{-4} Å^2)
	Nd–O(2)	4	2.31	70 ± 25	Ce–O(2)	4	2.21	40 ± 10
	Nd–O(1)	4	2.61	95 ± 40	Ce–O(1)	4	2.61	250 ± 100
	Nd–Cu	4	3.29	40 ± 15	Ce–Cu	4	3.34	50 ± 15
	Nd–Nd	4	3.65	60 ± 35	Ce–Nd(1)	4	3.66	40 ± 20
	Nd–Nd	4	3.88	25 ± 25	Ce–Nd(2)	4	3.91	100 ± 60

basal plane. Four more shells are identified, including Cu–Cu at $R = 3.94$ Å (using the MS approximation). The crystal structure of NACCO compounds is the same (T′-type) as in Nd_2CuO_4.

The data given in table 4 for the NACCO compounds indicate that the first-shell Ce–O(2) distance (2.24 Å) is shorter than the Nd–O(2) distance (2.31 Å). Interestingly, this Ce–O(2) distance is nearly the same as in NCCO (table 3), suggesting that co-doping with an alkaline earth element (Sr, Ca or Ba) has only a marginal effect on the Ce–O bond distance. The Ce–O bond distance in NACCO (and NCCO), on the basis of ionic radius considerations, matches reasonably with O^{2-}($r = 1.32$ Å) and Ce^{4+}($r = 0.88$ Å), while Ce^{3+}($r = 1.02$ Å) shows a large deviation. Further, the second-shell Nd–O(1) distance has rather high σ^2 value with large uncertainties. The other distances, Ce–Nd and Ce–Cu, in NACCO are nearly the same as those of Nd–Nd and Nd–Cu in Nd_2CuO_4, and the square symmetry of the O(2) first shell is also maintained around Ce in NACCO compounds.

The EXAFS data (table 4) clearly indicate that the Sr, Ca or Ba dopant occupies the Nd site in NACCO compounds. The square symmetry of O(2) is also maintained around Sr, Ca and Ba. The first-shell Sr–O(2), Ca–O(2) and Ba–O(2) bond distances (2.42, 2.26 and 2.66) match with the respective combinations of ionic radii of Sr^{2+}(1.12 Å), Ca^{2+}(0.99 Å) or Ba^{2+}(1.34 Å) with O^{2-}(1.32 Å). The Sr–, Ca– and Ba–cation distances are the same as for Nd.

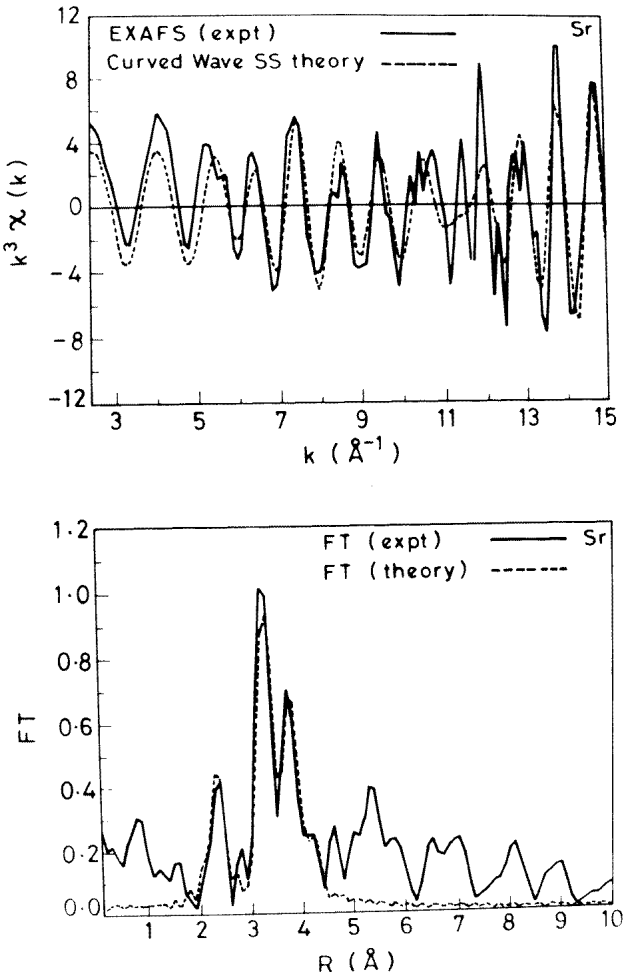

Figure 8. EXAFS (top) and FT (bottom) of Sr in NACCO ($z = 0.18$).

It is noted that while the first-shell oxygen, O(2), distances of Ce, Sr and Ca are short, both the first- and second-shell oxygen distances of Ba are very long. The second-shell oxygen, O(1), distance of Sr is the same as that of Nd but the second-shell Ca–O(1) distance is short, indicating that the O in the Cu–O layer moves. Thus, the Cu–O layer is distorted around the Ca atom. A similar distortion of the Cu–O layer around the Ba atom is inferred from the elongation of the second-shell Ba–O(1) bond length compared to Nd. This result is in fact as expected since the ionic radius of Ca^{2+} is shorter than that of Nd^{3+} while that of Ba^{2+} is much longer. The effect of doping is clearly seen on the local environments of the dopants (table 4). Interestingly, all the first-neighbour oxygen distances are consistent with the ionic radii [37].

The behaviour of O(1) in the Cu–O layer and the variation of Cu–O–Cu angle need some discussion. Figure 13 shows a layout of the T′-type layer structure. Layer A corresponds to Cu atoms defining coordinate $z = 0.00$; $z = 0.50$ is an equivalent layer or a mirror plane. The Nd atoms in Nd_2CuO_4 occupy layer B at $z = 0.15$; $z = 0.35$ is the equivalent

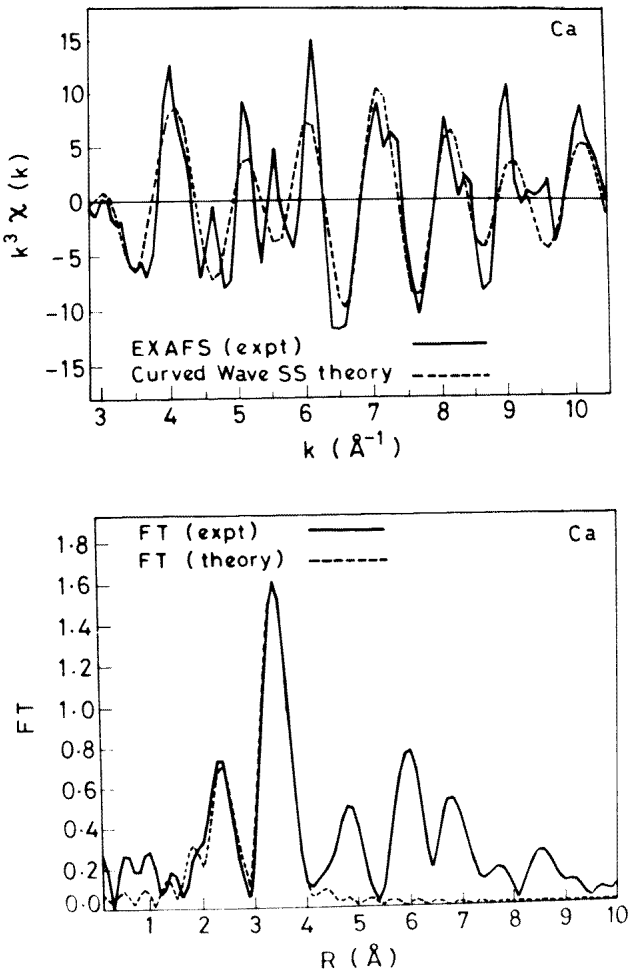

Figure 9. EXAFS (top) and FT (bottom) of Ca in NACCO ($z = 0.18$).

layer. A unit-cell diagram of the T′-type structure along with the Cu–O–Cu angle and bond distances is shown in figure 14. The positions of the in-plane oxygen O(1) and the out-of-plane oxygen O(2) are also marked in the figure following the notation of x-ray and neutron diffraction data [23–25].

Since the mean coordination number ($N = 4$) around the dopant ion is maintained and the dopant–cation distances remain the same as in Nd_2CuO_4, the dopants occupy layer B at $z = 0.15$ (Nd site). The oxygen O(2) is identified with layer C (figure 13). The dopant–O(2) distances vary and the z coordinate of O(2) also changes (table 5). The latter is found by triangulation using the cation–cation and cation–oxygen distances. The shifts in the dopant–O(2) distances are, generally, small except for Ba where the local shift in layer C is large. This may distort layer D (or the Nd layer) without affecting the Ba–Nd bond distance, which is the same as the lattice parameters computed from the diffraction data (table 1). Since Cu lies at $z = 0.00$ (always) and the dopant at $z = 0.15$, the Cu–O distances can vary if O(1) moves, thus distorting the Cu–O layer. Table 5 lists the oxygen z coordinate

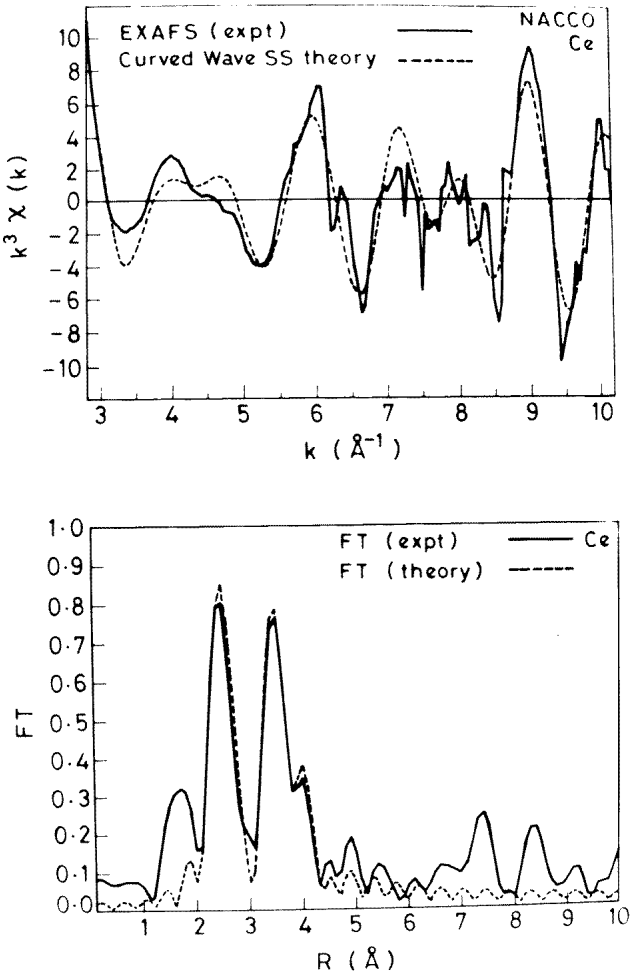

Figure 10. EXAFS (top) and FT (bottom) of Ce in NACCO ($z = 0.18$).

of O(1) in Cu–O layer. It is noted from the table that Ce and Sr as co-dopants (NACCO system) do not affect the planarity of the Cu–O layer, while Ca or Ba as a co-dopant with Ce distorts the Cu–O layer due to movement of the O(1) (figure 14).

In NACCO compounds the T_c depends on the alkaline earth dopant (see table 1). This, to some extent, can be correlated to movement of O(1) leading to distortion (non-coplanarity) of the Cu–O layer. On co-doping, the local environments of Sr and Ce in NACCO compounds are similar and the Cu–O layers are square planar. On the other hand, the local environments of Ba or Ca are significantly different from those of Sr and Ce, and the Cu–O layers no longer remain square planar. The Cu–O–Cu angle shows large deviation from linearity ($\sim 180^\circ$) on Ba or Ca co-doping with Ce in NACCO compounds. It is apparent from the data (table 5) that the Cu–O–Cu angle changes from $\sim 177 \pm 10^\circ$ (for Nd_2CuO_4) to $175 \pm 10^\circ$ on Ce doping and it falls further to $160 \pm 10^\circ$ on doping with Ce+Ca or Ce+Ba (see figure 14). The Ce+Sr doping, however, recovers the Cu–O–Cu angle to near linearity ($174 \pm 10^\circ$). Thus doping Sr in non-SC $Nd_{1.82}Ce_{0.18}CuO_y$ samples

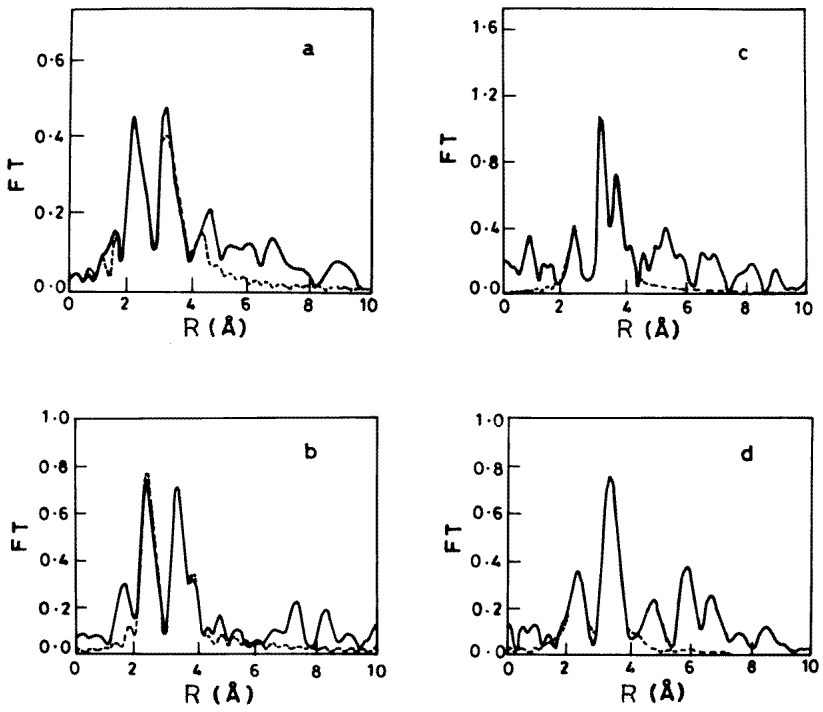

Figure 11. FTs of EXAFS of (a) Nd in Nd_2CuO_4, (b) Ce in NACCO (A = Ca and $z = 0.18$), (c) Sr in NACCO (A = Sr and $z = 0.06$) and (d) Ca in NACCO (A = Ca and $z = 0.18$).

leads to a more congenial environment leading to revival of T_c to 23 K, which is close to the maximum value of T_c (24 K) observed for the T′-type (NCCO, $x = 0.15$) compound. For the cases of Ce+Ca or Ce+Ba doped samples, wherein the Cu–O–Cu angle deviation from linearity is large, T_c is also revived, albeit to lower values (see table 1). Thus, the results suggest that in NACCO T′-type compounds non-linearity of Cu–O–Cu bonds and non-co-planarity of Cu and O(1) adversely affect T_c due to weakening of the Cu 3d–O 2p effective overlap.

In summary it is found that in Nd_2CuO_4 the Cu site is well ordered and the Cu–O–Cu angle is nearly linear ($177 \pm 10^\circ$). The local structure is sensitive to Ce doping. However, the Cu–O bond rigidity is somewhat weakened (increase in σ^2) on Ce doping. This enables creation of oxygen vacancies/point defects in the NCCO compound on reduction annealing (as the observed Cu–O coordination is less than four), leading to increase in the carrier (electron) density and local structural modifications essential for the NCCO samples to exhibit superconductivity. It appears that the lower values of N (< 4) point toward local structural configurations that facilitate the stabilization of a small quantity of interstitial/apical oxygen O(3) in the proximity of Ce^{4+} in the SC NCCO compound.

In $Ce_{0.18}$-NCCO samples, the higher content of Ce (Ce^{4+} predominant) with strong affinity for oxygen near neighbours inhibits the creation of oxygen vacancies even on reduction annealing [11] and causes the samples to be non-SC [12]. The T_c is, however, revived [7] (see figure 2) in the Ce(0.18) sample when it is co-doped with divalent Sr ($z = 0.06$) followed by reduction annealing that causes creation of some, albeit a low level of, oxygen vacancies [11]. The Sr and Ce environments are found to be similar

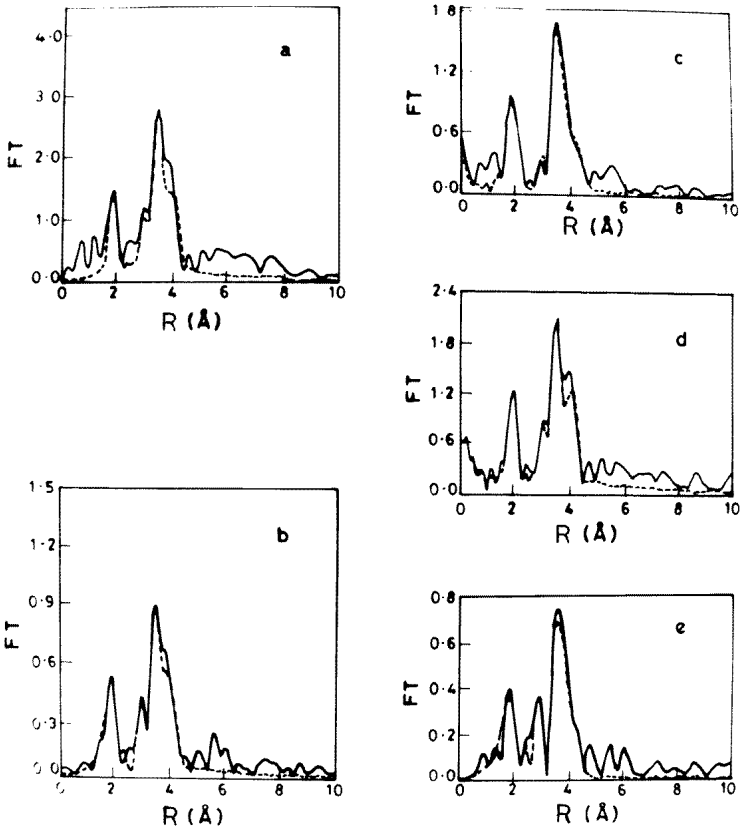

Figure 12. FTs of EXAFS of Cu in (a) Nd_2CuO_4, (b) $Nd_{1.85}Ce_{0.15}CuO_{3.97}$, (c) $Nd_{1.64}Ca_{0.18}Ce_{0.18}CuO_y$, (d) $Nd_{1.64}Ba_{0.18}Ce_{0.18}CuO_y$ and (e) $Nd_{1.64}Sr_{0.18}Ce_{0.18}CuO_y$.

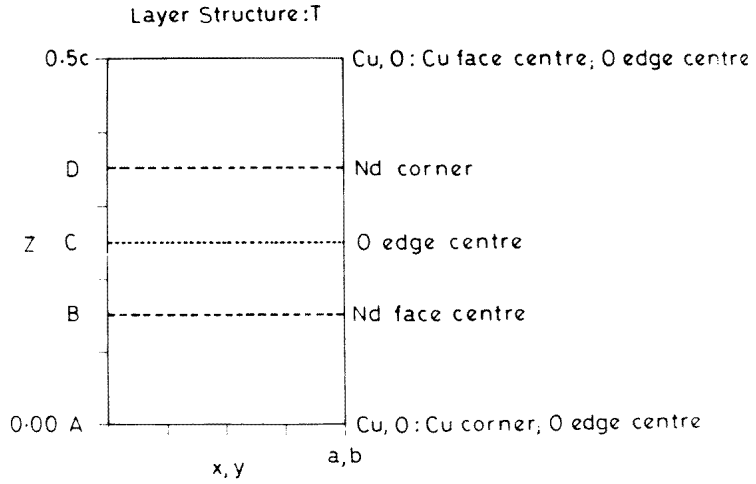

Figure 13. The layout of the T′-type layer structure.

Table 4. R, N and σ^2 values as obtained from EXAFS analysis for $Nd_{1.82-z}A_zCe_{0.18}CuO_y$ (NACCO). Co-ordination numbers are held fixed.

		EXAFS (present)			XRD		
	Bond	R	ΔR	σ^2	$\Delta\sigma^2$	N	R
Mean Cu environment							
	Cu–O(1)	1.96	0.02	40	20	4	1.969
	Cu–Nd	3.31	0.04	50	40	8	3.328
	Cu–O(2)	3.61	0.08	50	50	8	3.620
	Cu–Cu	3.94	0.04	50	50	4	3.939
Mean Nd environment							
	Nd–O(2)	2.31	0.04	70	30	4	2.324
	Nd–O(1)	2.65	0.04	50	50	4	2.671
	Nd–Cu	3.30	0.02	90	50	4	3.328
	Nd–Nd(1)	3.69	0.04	100	50	4	3.720
	Nd–Nd(2)	3.90	0.04	80	60	4	3.939

Ce environment				Sr environment			
Bond	N	R(±0.02 Å)	$\sigma^2(10^{-4}$ Å$^2)$	Bond	N	R (Å)	$\sigma^2(10^{-4}$ Å$^2)$
Ce–O(2)	4	2.24	40 ± 30	Sr–O(2)	4	2.40	50 ± 20
Ce–O(1)	4	2.63	150 ± 100	Sr–O(1)	4	2.62	80 ± 40
Ce–Cu	4	3.34	50 ± 20	Sr–Cu	4	3.28	60 ± 30
Ce–Nd(1)	4	3.69	60 ± 20	Sr–Nd(1)	4	3.76	30 ± 30
Ce–Nd(2)	4	3.92	100 ± 20	Sr–Nd(2)	4	3.94	50 ± 50

Ca environment				Ba environment			
Bond	N	R (Å)	$\sigma^2(10^{-4}$ Å$^2)$	Bond	N	R (Å)	
Ca–O(2)	4	2.26	60	Ba–O(2)	4	2.66	
Ca–O(1)	4	2.42	30	Ba–O(1)	4	2.82	
Ca–Cu	4	3.31	30	Ba–Cu	4	3.35	
Ca–Nd(1)	4	3.51	20	Ba–Nd(1)	4	3.68	
Ca–Nd(2)	4	3.76	150	Ba–Nd(2)	4	3.93	

ΔR and $\Delta\sigma^2$ are the ranges of values found in different samples.
Absolute uncertainties $R \pm 0.02$ Å; $\sigma^2 \pm 50 \times 10^{-4}$ Å^2.

and the planarity of the Cu–O layer is not affected. The contracted Ce–O(2) bond distance ($R = 2.24 \pm 0.02$ Å) is regained on co-doping with Sr; the Sr–O(2) distance ($R = 2.38 \pm 0.02$ Å) is marginally longer. The spatial symmetry of the local environment of Ca or Ba dopant is, however, different from those of Ce and Sr. Ca doping shortens the Ca–O(2) distance while Ba doping elongates the bond lengths, thereby distorting the Cu–O layer. The effects of such variations in local structure of Cu–O are reflected in the observed decrease in T_c values for these compounds (table 1).

5. Conclusions

The results of EXAFS studies on the T′-type Nd based cuprates lead to the following conclusions. (i) Ce alone, and Ba, Ca or Sr with Ce as co-dopant, substitute for Nd without distorting the overall T′ structure. (ii) For Cu EXAFS, the small-atom multiple-scattering theory gives a better fit than the curved wave theory in the single-scattering approximation. This clearly indicates that Cu–Cu bonds along the a (or b) axis contain a strong multiple-

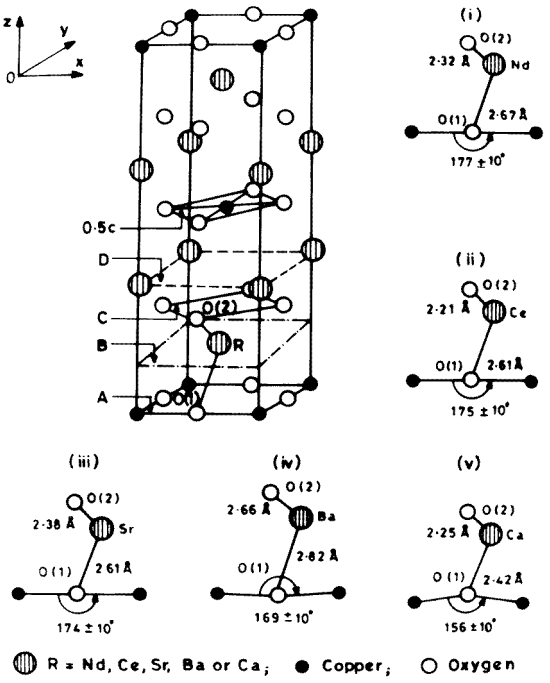

Figure 14. A schematic diagram of the unit cell of the T′-type structure showing different layers A–D. Effect of doping on the Cu–O–Cu angle is illustrated: O(1) is the in-plane and O(2) is the out-of-plane oxygen.

Table 5. Dopant–O(2) distance: O(2) is the out-of-plane oxygen. Layer C position: dopant is at $z = 0.15$, with unperturbed oxygen at $z = 0.25$. Oxygen in the Cu–O layer position with Cu at $z = 0.00$: O(1) is the in-plane oxygen. The z value is determined by triangulation (see the text for details) and the bond angle from fitting including multiple-scattering contributions.

Ion	R (O(2)) (Å)	z (O(2))		
Nd	2.31	0.250		
Ce	2.24	0.238		
Ba	2.66	0.298		
Ca	2.26	0.241		
Sr	2.42	0.263		
	R (O(1)) (Å)	z (O(1))	Cu–O–Cu (±10°)	Cu–O layer
Nd	2.65	0.004	177	planar
Ce	2.63	0.007	175	planar
Ba	2.82	−0.016	169	distorted
Ca	2.42	0.034	156	distorted
Sr	2.62	0.008	174	planar

scattering contribution. (iii) Ce doping in Nd_2CuO_4 weakens the planar Cu–O bond and on reduction causes oxygen depletion ($N < 4$) essential for superconductivity. (iv) In the

NACCO samples, Ce and Sr co-doping does not distort the Cu–O layer while its distortion is found in the cases of Ca and Ba co-doped with Ce samples wherein T_c values are low, indicating the adverse effect of non-coplanarity of the Cu–O layer on T_c. (v) A clear indication of a small amount of oxygen at the interstitial/apical oxygen, O(3), position is found in the SC samples. This raises a moot point if apical oxygen is essential in T′ cuprates to exhibit superconductivity. Finally, the present studies have clearly shown the potentialities of the EXAFS technique in probing the local structure.

Acknowledgments

We wish to thank the UK SERC for the provision of synchrotron beam time. One of us (BDP) acknowledges financial support from CSIR New Delhi. Thanks are also due to S Gupta, R Suba and R D Kale for their help.

References

[1] Tokura Y, Takagi H and Uchida S 1989 *Nature* **337** 345
[2] Takagi H, Uchida S and Tokura Y 1989 *Phys. Rev. Lett.* **62** 1197
[3] Stadlober B, Kurg G, Nemetschek R, Hackl R, Cobb J L and Markert J T 1995 *Phys. Rev. Lett.* **74** 4911
[4] Liang G, Guo Y, Badresing D, Xu W, Tang Y, Croft M, Chen T, Sahiner A, Beom-hoan O and Markert J T 1995 *Phys. Rev.* B **51** 1258
[5] Brinkmann M, Rex T, Bach H and Westerholt L 1995 *Phys. Rev. Lett.* **75** 4927
[6] Ghigna P, Spinolo G, Scavani M, Anselmi T U and Chadwick A V 1995 *Physica* C **253** 147
[7] Singh O G, Om Prakash, Padalia B D and Narlikar A V 1993 *Phys. Rev.* B **48** 13 182
[8] Singh O G 1995 *PhD Thesis* Indian Institute of Technology
[9] Jiang W, Mao S N, Xi X X, Jiang X, Peng J L, Venkatesan T, Lobb C J and Greene R L 1994 *Phys. Rev. Lett.* **73** 1291
[10] Seffar A, Fontcuberta J, Pinol S, Obradors X, Peraudeau G and Berjoan R 1996 *Physica* C **259** 75
[11] Singh O G, Harendranath C S, Om Prakash and Padalia B D 1996 *Solid State Commun.* **100** 721
[12] Singh O G, Padalia B D, Om Prakash, Suba K, Narlikar A V and Gupta L C 1994 *Physica* C **219** 156
[13] Brugger T, Schreiner T, Roth G, Adelmann P and Czjzek G 1993 *Phys. Rev. Lett.* **71** 2481–4
[14] Sumarlin I W, Lynn J W, Neumann D A, Rush J J, Loong C K, Peng J L and Li Z Y 1993 *Phys. Rev.* B **48** 473
[15] Okram G S, Om Prakash, Padalia B D, Chandrasekharam D, Tamhane A S and Gupta L C 1992 *Supercond. Sci. Technol.* **5** 561
[16] Paulus E F, Yehia I, Fuess H, Rodriguez J, Vogt T, Strobel J, Klauda M and Saemann-Ischenko G 1990 *Solid State Commun.* **73** 791
[17] Shen Z X, Spicer W E, King D M, Dessau D S and Wells B O 1995 *Science* **267** 343
[18] Singh O G, Padalia B D, Om Prakash, Agarwal S K and Narlikar A V 1996 *J. Appl. Phys.* **80** 5169
[19] Padalia B D, Singh O G, Om Prakash, Gurman S J and Amiss J C 1995 *Physica* B **208/209** 531
[20] Li G G, Bridges F, Boyce J B and Joiner W C H 1993 *Phys. Rev.* B **47** 12 110
[21] Padalia B D, Gurman S J, Mehta P K and Om Prakash 1992 *J. Phys.: Condens. Matter* **4** 6865
[22] Zhengquan T, Budnick J I, Peng J L, Lu Z and Shelter R N 1993 *Physica* B **163** 13
[23] Muller-Buschbaum V H and Wollschlager W 1975 *Z. Anorg. (Allg.) Chem.* **414** 76
[24] Izumi F, Matsui Y, Takagi H, Uchida S, Tokura Y and Asano H 1989 *Physica* C **158** 433
[25] Kajitani T, Hiraga K, Hosoya S, Fukuda T, Ishi-O, Kikuchi M, Syono Y, Tomiyoshi S, Takahashi M and Muto Y 1990 *Physica* **169** 227
[26] Kwei G H, Cheong S W, Fisk Z, Garzon F H, Goldstone J A and Thompson J D 1989 *Phys. Rev.* B **40** 9370
[27] Radaelli P G, Jorgensen J D, Schultz A Z, Peng J L and Greene R L 1994 *Phys. Rev.* B **49** 15 322
[28] Morrell C, Baines J T M, Campbell J C, Diakun G P, Dobson B R, Greaves G and Hasnain S S *Daresbury EXAFS User's Manual* (Daresbury: SERC Daresbury Laboratory) undated
[29] Gurman S J, Binsted N and Ross I 1984 *J. Phys. C: Solid State Phys.* **17** 143
[30] Binsted N, Gurman S J, Campbell T C and Stephenson P C 1992 *EXCURV92 Program* (Daresbury: SERC Daresbury Laboratory)
[31] Hedin L and Lundqvist B 1971 *J. Phys. C: Solid State Phys.* **4** 2347

[32] Gurman S J, Diakun G, Dobson B, Abell S, Greaves G N and Jordan R 1988 *J. Phys. C: Solid State Phys.* **21** L475, and references therein
[33] Joyner R W, Martin K J and Meehan P 1987 *J. Phys. C: Solid State Phys.* **20** 4005
[34] Ghigna P, Spinolo G, Filipponi A, Chadwick A V and Hanmer P 1995 *Physica* C **246** 345
[35] Marin C, Henry J Y and Boucherle J X 1993 *Solid State Commun.* **86** 425
[36] Padalia B D, Singh O G, Gurman S J, Suba K and Om Prakash 1995 *Physica* C **208/209** 533
[37] Shannon R D 1976 *Acta Crystallogr.* A **32** 751